Sites Contributing to TRPA1 Activation by the Anesthetic Propofol Identified by Photoaffinity Labeling

Sites Contributing to TRPA1 Activation by the Anesthetic Propofol Identified by Photoaffinity Labeling

Kellie A. Woll,*[a] Kenneth A. Skinner,†[a] Eleonora Gianti,‡ Natarajan V. Bhanu,¶ Benjamin A. Garcia,¶ Vincenzo Carnevale,‡ Roderic G. Eckenhoff,* and Rachelle Gaudet†

*Department of Anesthesiology & Critical Care, University of Pennsylvania Perelman School of Medicine, 3620 Hamilton Walk, Philadelphia, PA, USA.; †Molecular and Cellular Biology; Harvard University, Cambridge, MA USA.; ‡Institute for Computational Molecular Science, Department of Chemistry;Temple University, Philadelphia, PA, USA.; ¶ Epigenetics Program, Department of Biochemistry and Biophysics, Perelman School of Medicine, University of Pennsylvania, PA, USA.

[a]Contributed equally

ABSTRACT In addition to inducing anesthesia, propofol activates a key component of the pain pathway, the transient receptor potential ankyrin 1 ion channel (TRPA1). Recent mutagenesis studies suggested a potential activation site within the transmembrane domain near the A-967079 cavity. However, mutagenesis cannot distinguish between protein-based and ligand-based mechanisms, nor can this site explain the complex modulation by propofol. Thus more direct approaches are required to reveal potentially druggable binding sites. Here we apply photoaffinity labeling using a propofol derivative, *meta*-azipropofol (AziP*m*), for direct identification of binding sites in mouse TRPA1. We confirm that AziP*m* activates TRPA1 like the parent anesthetic, and identify two photolabeled residues (V954 and E969) in the S6 helix. In combination with docking to closed and open state models of TRPA1, photoaffinity labeling suggested that the A-967079 cavity is a positive modulatory site for propofol. Furthermore the photoaffinity labeling of E969 indicated pore block as a likely mechanism for propofol inhibition at high concentrations. The direct identification of drug binding sites clarifies the molecular mechanisms of important TRPA1 agonists and will facilitate drug design efforts to modulate TRPA1.

Received for publication "Staff will complete" and in final form "Staff will complete"

Address reprint requests and inquiries to: R. Gaudet & R. G. Eckenhoff

Transient receptor potential (TRP) ion channels constitute a 28-member family mainly composed of outwardly rectifying, nonselective cation channels and are commonly considered to be detectors and transducers of sensory stimuli (1). TRP Ankyrin 1 (TRPA1) represents the lone member of the TRPA subfamily within mammals (2). Although primarily associated with nociception (3, 4), TRPA1 also influences physiological functions other than pain sensing (5).

TRPA1 is primarily considered a chemosensor; it has a long list of endogenous and exogenous agonists and antagonists (1, 2). The agonists can be divided into either electrophilic or non-electrophilic modulators (6). Interestingly some general anesthetics are TRPA1 non-electrophilic agonists, resulting in paradoxical *pro*-nociceptive effects (7–10). For example, propofol (Figure 1A), the most commonly used intravenous general anesthetic, shows a bimodal activity on TRPA1; activating at low concentration and blocking at high (7, 9). Studies have shown that TRPA1 is the major player in propofol's algogenic properties, as well as a potential contributor to post-operative pain and propofol-induced vasodilation (7, 11). As our understanding of the channel's physiological functions improves, it becomes progressively clearer that the activation/inhibition of TRPA1 may also influence other aspects of propofol pharmacology including those that may directly underlie components of anesthesia.

Uncovering the propofol modulatory site(s) will further our understanding of the TRPA1 molecular machinery and physiological functions as well as provide information for drug design. Ton *et al*. identified a series of mutations (S876V, S876V/T877L, M915L or M956A/V) that eradicated propofol activation of rat TRPA1 (12). These studies suggested a binding cavity, common with the TRPA1 antagonist A-967079 site (12, 13), as an allosteric site for propofol modulation. However site-directed mutagenesis cannot definitively distinguish ligand binding sites from confounding alterations in the protein's dynamics. Therefore more direct approaches are needed to reveal the propofol binding site(s) in TRPA1. We used photoaffinity labeling, using a photoactive derivative of propofol called *meta*-azipropofol (AziP*m*; Figure 1A) (14) to provide direct evidence for alkylphenol-based anesthetic binding sites within heterogously expressed mouse TRPA1.

To allow for photoreactivity, modifications within the propofol chemical structure were required (14). AziP*m* contains a trifluorodiazirine at the *meta*-position that upon UV irradiation generates a singlet carbene, a highly reactive and photochemically nonselective species (15, 16). As a result, AziP*m* provides for unbiased labeling of binding sites. However, given the differences in their chemical structures, we first aimed to verify that AziP*m* demonstrated similar TRPA1 activity as compared to the parent anesthetic propofol. To accomplish this we

measured activation of C-terminally tagged mouse TRPA1 (*m*TRPA1-FLAG) expressed baculovirus-infected Sf21 insect cells using a Fura-2 based bulk calcium influx assay. Both propofol and AziP*m* significantly activated *m*TRPA1 channels within concentration ranges similar to those used for propofol in previous reports (see Fig. S1) (7, 9, 12). The responses to both propofol and AziP*m* were specific to *m*TRPA1 as neither caused calcium influx in rat TRP vanilloid 1 (*r*TRPV1)-expressing or empty-vector baculovirus-infected Sf21 cells (see Fig. S1). *m*TRPA1-FLAG activation was concentration dependent (see Fig. S1) with EC_{50} values of 17 μM (11.7-25.0 μM; CI 95%) and 8.1 μM (3.18-26.1 μM; CI 95%) for propofol and AziP*m* respectively (see Supporting Materials and Methods). The activating concentrations are considered clinically relevant (0.3-60 μM) (17, 18) and are comparable to other established protein targets like $GABA_A$ receptors (19). Also similar to previous reports, both propofol and AziP*m* exhibited bimodal effects, with reduced activation at the highest concentration examined (see Fig. S1) (7, 9). In summary, the similar modulatory behavior of both propofol and the photoaffinity derivative AziP*m* likely reflect shared TRPA1 binding site(s).

Next we sought to determine whether the similar TRPA1 functional activity displayed by AziP*m* was via common binding site(s) with propofol. To this end, isolated membranes containing *m*TRPA1-FLAG were photolabeled with tritiated AziP*m* ([^{3}H]AziP*m*) in the presence or absence of propofol. After photolabeling, channels were purified using anti-FLAG resin and SDS-PAGE electrophoresis. We then determined whether the propofol inhibited, or 'protected', (15) *m*TRPA1-FLAG binding sites from [^{3}H]AziP*m* photoradiolabeling by scintillation counting. The use of radiolabeling allows for a semi-quantitative assessment of propofol's protection of shared binding sites from the irreversible [^{3}H]AziP*m* photolabeling (15). Propofol decreased [^{3}H]AziP*m* photoincorporation by 53% (Fig. 1B), similar to what has been observed within other known propofol targets (15, 16), including the $GABA_A$ receptor (19). Therefore, the result is consistent with our functional results that suggested common binding site(s) and molecular mechanism.

We next identified the *m*TRPA1-FLAG residues photolabeled with AziP*m* by mass spectrometry (MS) microsequencing. After photolabeling isolated membranes containing *m*TRPA1-FLAG, we purified the channels using anti-FLAG resin and SDS-PAGE electrophoresis followed by in-gel sequential trypsin and chymotrypsin digestion. MS analysis resulted in ~93% sequence coverage (see Fig. S2) two residues with the AziP*m* photomodification were detected: V954 and E969 (Figure 2C, see Fig S3-4). Both residues are located within a highly conserved region of the TRPA1 S6 helix in the TMD and are identical for both *m*TRPA1 and human TRPA1 (*h*TRPA1; Figure 2D). S6, along with S5, forms the channel gate within 6TM-channels; therefore it is not surprising that ligand binding near S6 influences the dynamics and activity of 6TM-channels (20, 21). Interestingly these residues do not share identity within the propofol insensitive *Drosophila* TRPA1 (9, 12), again suggesting that these residues may contribute to functionally relevant propofol binding site(s) (Figure 2D). Of note, the two residues are not exposed to a shared cavity; the structure instead suggests that each label corresponds to a distinct binding site on TRPA1.

To further clarify the propofol and AziP*m* binding cavities that contribute to the altered activity, we generated models of *h*TRPA1 in the closed state (model-1) and open state (model-2). The available *h*TRPA1 electron cryomicroscopy (cryo-EM) structure (PDB: 3J9P) is anticipated to represent an intermediate state displaying a likely open upper and closed lower channel gates (13). Model-1 shows the upper gate in a closed conformation while model-2 shows an open upper and lower hydrophobic gate with a continuous pore diameter sufficient to allow passage of partially dehydrated calcium ions (>6 Å) (13, 22) (see Fig. S5). The photolabeled residues V954 and E969 in *m*TRPA1-FLAG align with V951 and E966 respectively in *h*TRPA1 (Figure 2D). E966 is located near the end of the S6 helix below the lower hydrophobic gate defined by I957 and V961. Within model-2 the S6 helices adopt a 'bend and twist' conformation in comparison to the cryo-EM structure, an anticipated common conformational change for opening of 6TM-channels (23, 24), which orients E966 more fully into pore (Fig 2D-E). Given the location of the photolabeled residue respective to the lower hydrophobic gate and putative open state model, we anticipate that the E969 photolabeling in *m*TRPA1-FLAG by AziP*m* is indicative of an activation-dependent pore block site. Indeed propofol and AziP*m* both displayed similar bimodal activity (see Fig S1) and propofol has been reported to display a 'surge' response during drug wash out, characteristic of pore block inhibition (7, 9).

Within model-1 and model-2, V951 is located on the S6 helix near two previously reported ligand binding pockets within TRP channels (2): the S4-S5 pocket, analogous to the resiniferatoxin binding site in rat TRPV1 (24), and the S5-S6 pocket containing the antagonist A-967079 site (13). Model-1 orients V951 facing the S4-S5 linker and therefore accessible to both pockets while the conformation adopted in model-2 orients the residue further into the S5-S6 pocket (Fig. 2B-C). We performed docking experiments using AutoDockVina (25) and set a docking region that included both cavities to elucidate whether propofol and AziP*m* would be capable of occupying either pocket. The results indicated that for both models the S4-S5 and S5-S6 pockets could accommodate either ligand with poses represented in either site. For both model-1 and model-2 the highest scored and the majority of docking poses were located

within the S5-S6 pocket near the A-967079 binding site (13) and in close proximity to the V951 (Fig. 2B-C). Recently it has been shown that mutating S876, S876/T877, M915 or M956 in *m*TRPA1 selectively abolishes propofol activation of the channel (12). These residues align with S873, T874, M912, and M953 in *h*TRPA1 and indicated a propofol allosteric site within the S5-S6 pocket. Our results showing the photolabeling of V954 in *m*TRPA1 by AziP*m* confirms a likely positive modulatory anesthetic binding site within the TRPA1 TMD and further suggests the S5-S6 as an activation site for propofol.

Cumulatively our results suggest that: (i) propofol *activation* of TRPA1 is through a higher affinity binding site located within TMD cavities associated with the S6 helix, likely within the S5-S6 pocket, and (ii) propofol *inhibition* of TRPA1 at higher concentrations is by activation-dependent pore block, likely proximal to E969. Together these mechanisms would be predicted to result in the observed bimodal TRPA1 activity. Given the lack of current structural knowledge, specifically on the open state channel, determining an exact molecular mechanism is a challenge. To glean insights into the molecular determinants of such state-dependent binding of propofol, we generated a model of TRPA1 open state using the cryo-EM structure of TRPV1 as template. Due to the uncertainties inherent to comparative homology modeling, we regard the resulting structural information as hypothetical. Within these limitations, docking simulations show that, in the open state, V951 and E969 are oriented toward a potential positive modulatory site and the conduction pore, respectively, thereby providing a tentative explanation for the dual effect of propofol.

Two complementary but distinct approaches, mutagenesis (12) and photolabeling studies described here, suggest a propofol activation site located within the S5-S6 pocket of TRPA1. Additionally, our current and other previous investigations show that propofol, at high concentrations, has functional activity that is characteristic of non-specific pore block (7, 9). Our study provides additional support for this mechanism by the identification of a second photolabeled site within the TRPA1 pore.

Each approach has limitations. Photolabeling requires a modified ligand and the inability to link each site to a specific functional role. Mutagenesis alone often results in ambiguity because of changes to protein dynamics and energetics unrelated to ligand binding. Taken together, however, our methods and results directly identify alkylphenol-based general anesthetic binding sites on TRPA1 receptors that rationally explain both activation and inhibition of ion channel activity, and that furthers our understanding of the pharmacology of these commonly used drugs.

SUPPORTING MATERIAL

Supporting Materials and Methods and five figures are available online at:

AUTHOR CONTRIBUTIONS

K.A.W., K.A.S., E.G., N.B., B.A.G, V.C., R.G.E., and R.G. contributed to research design; K.A.W., K.A.S., E.G., and N.B. contributed to the conduction of experiments; K.A.W., K.A.S., and E.G., conducted data analysis; K.A.W., K.A.S., E.G., V.C., R.G.E., and R.G. contributed to the writing of the manuscript.

ACKNOWLEDGEMENTS

We thank David A. Solá-Del Valle and Christopher B. Phelps for generating the mTRPA1-FLAG bacmid, and Hitoshi Inada and A. Ertugrul Cansizoglu for help optimizing the calcium-influx assay and TRPA1 proteolysis, respectively. This work was supported by the American Heart Association (16GRNT27250119), the National Institutes of Health (GM055876, GM107117, GM110174), and the Department of Defense (BC123187P1). K.A.S. was supported by an NSF Graduate Research Fellowship (DGE-1144152) and a Ford Foundation Fellowship.

CONFLICT OF INTEREST

Authors declare no conflict of interest.

REFENENCES

1. Mickle, A.D., A.J. Shepherd, and D.P. Mohapatra. 2015. Sensory TRP channels: the key transducers of nociception and pain. Prog. Mol. Biol. Transl. Sci. 131: 73–118.
2. Brewster, M.S.J., and R. Gaudet. 2015. How the TRPA1 receptor transmits painful stimuli: Inner workings revealed by electron cryomicroscopy. Bioessays. 37: 1184–1192.
3. Uta, D., H. Furue, A.E. Pickering, M.H. Rashid, H. Mizuguchi-Takase, T. Katafuchi, K. Imoto, and M. Yoshimura. 2010. TRPA1-expressing primary afferents synapse with a morphologically identified subclass of substantia gelatinosa neurons in the adult rat spinal cord. Eur. J. Neurosci. 31: 1960–1973.
4. Barabas, M.E., E.A. Kossyreva, and C.L. Stucky. 2012. TRPA1 is functionally expressed primarily by IB4-binding, non-peptidergic mouse and rat sensory neurons. PLoS One. 7: e47988.
5. Fernandes, E.S., M.A. Fernandes, and J.E. Keeble. 2012. The functions of TRPA1 and TRPV1: moving away from sensory nerves. Br. J. Pharmacol. 166: 510–521.
6. Laursen, W.J., S.N. Bagriantsev, and E.O. Gracheva. 2014. TRPA1 channels: chemical and temperature sensitivity. Curr. Top. Membr. 74: 89–112.
7. Matta, J.A., P.M. Cornett, R.L. Miyares, K. Abe, N. Sahibzada, and G.P. Ahern. 2008. General

anesthetics activate a nociceptive ion channel to enhance pain and inflammation. Proc. Natl. Acad. Sci. U. S. A. 105: 8784–8789.

8. Mutoh, T., Y. Taki, and H. Tsubone. 2013. Desflurane but not sevoflurane augments laryngeal C-fiber inputs to nucleus tractus solitarii neurons by activating transient receptor potential-A1. Life Sci. 92: 821–828.
9. Fischer, M.J.M., A. Leffler, F. Niedermirtl, K. Kistner, M. Eberhardt, P.W. Reeh, and C. Nau. 2010. The general anesthetic propofol excites nociceptors by activating TRPV1 and TRPA1 rather than GABAA receptors. J. Biol. Chem. 285: 34781–34792.
10. Lee, S.P., M.T. Buber, Q. Yang, R. Cerne, R.Y. Cortes, D.G. Sprous, and R.W. Bryant. 2008. Thymol and related alkyl phenols activate the hTRPA1 channel. Br. J. Pharmacol. 153: 1739–1749.
11. Sinha, S., P. Sinharoy, I.N. Bratz, and D.S. Damron. 2015. Propofol causes vasodilation in vivo via TRPA1 ion channels: role of nitric oxide and BKCa channels. PLoS One. 10: e0122189.
12. Ton, H.T., T.X. Phan, A.M. Abramyan, L. Shi, and G.P. Ahern. 2017. Identification of a putative binding site critical for general anesthetic activation of TRPA1. Proc. Natl. Acad. Sci. U. S. A. .
13. Paulsen, C.E., J.-P. Armache, Y. Gao, Y. Cheng, and D. Julius. 2015. Structure of the TRPA1 ion channel suggests regulatory mechanisms. Nature. 520: 511–517.
14. Hall, M.A., J. Xi, C. Lor, S.P. Dai, R. Pearce, W.P. Dailey, and R.G. Eckenhoff. 2010. m-Azipropofol (AziPm) a Photoactive Analogue of the Intravenous General Anesthetic Propofol. J. Med. Chem. 53: 5667–5675.
15. Woll, K.A., W.P. Dailey, G. Brannigan, and R.G. Eckenhoff. 2016. Shedding Light on Anesthetic Mechanisms: Application of Photoaffinity Ligands. Anesth. Analg. 123: 1253–1262.
16. Weiser, B.P., K.A. Woll, W.P. Dailey, and R.G. Eckenhoff. 2014. Mechanisms revealed through general anesthetic photolabeling. Curr Anesth. Rep. 4: 57–66.
17. Franks, N.P., and W.R. Lieb. 1994. Molecular and cellular mechanisms of general anaesthesia. Nature. 367: 607–614.
18. Sall, J.W., G. Stratmann, J. Leong, E. Woodward, and P.E. Bickler. 2012. Propofol at clinically relevant concentrations increases neuronal differentiation but is not toxic to hippocampal neural precursor cells in vitro. Anesthesiology. 117: 1080–1090.
19. Jayakar, S.S., X. Zhou, D.C. Chiara, Z. Dostalova, P.Y. Savechenkov, K.S. Bruzik, W.P. Dailey, K.W. Miller, R.G. Eckenhoff, and J.B. Cohen. 2014. Multiple Propofol Binding Sites in a gamma-Aminobutyric Acid Type A Receptor (GABAAR) Identified Using a Photoreactive Propofol Analog. J Biol Chem. 1: 27456–27468.
20. Christopoulos, A., J.-P. Changeux, W.A. Catterall, D. Fabbro, T.P. Burris, J.A. Cidlowski, R.W. Olsen, J.A. Peters, R.R. Neubig, J.-P. Pin, P.M. Sexton, T.P. Kenakin, F.J. Ehlert, M. Spedding, and C.J. Langmead. 2014. International Union of Basic and Clinical Pharmacology. XC. multisite pharmacology: recommendations for the nomenclature of receptor allosterism and allosteric ligands. Pharmacol. Rev. 66: 918–947.
21. Bu, W., Q. Liang, L. Zhi, L. Maciunas, P.J. Loll, R.G. Eckenhoff, and M. Covarrubias. 2017. Sites and Functional Consequence of Alkylphenol Anesthetic Binding to Kv1.2 Channels. Mol. Neurobiol. .
22. Voets, T., A. Janssens, G. Droogmans, and B. Nilius. 2004. Outer pore architecture of a Ca2+-selective TRP channel. J. Biol. Chem. 279: 15223–15230.
23. Catterall, W.A. 2014. Structure and Function of Voltage-Gated Sodium Channels at Atomic Resolution. Exp. Physiol. 99: 10.1113/expphysiol.2013.071969.
24. Gao, Y., E. Cao, D. Julius, and Y. Cheng. 2016. TRPV1 structures in nanodiscs reveal mechanisms of ligand and lipid action. Nature. 534: 347–351.
25. Trott, O., and A.J. Olson. 2010. AutoDock Vina: improving the speed and accuracy of docking with a new scoring function, efficient optimization, and multithreading. J. Comput. Chem. 31: 455–61.
26. Trott, O., and A.J. Olson. 2010. Software News and Update AutoDock Vina: Improving the Speed and Accuracy of Docking with a New Scoring Function, Efficient Optimization, and Multithreading. J. Comput. Chem. 31: 455–461.

FIGURES

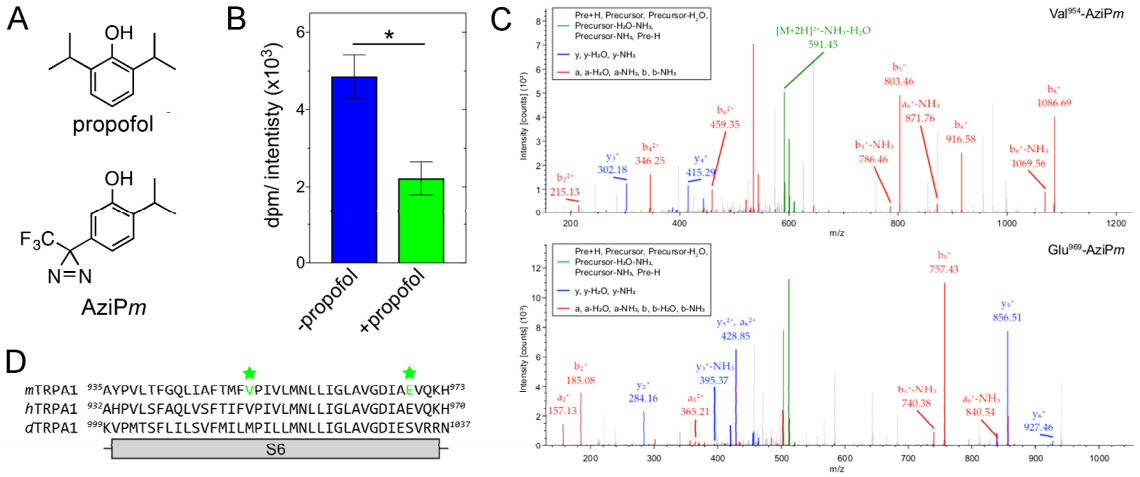

FIGURE 1. Mouse TRPA1-FLAG channel (*m*TRPA1-FLAG) photoaffinity labeled by AziP*m*. (A) Chemical stuctures of propofol and *meta*-azipropofol (AziP*m*). (B) Protection by propofol (100 μM) from photoaffinity labeling of *m*TRPA1-FLAG in Sf21 cell membranes with 1 μM [^{3}H]AziP*m*. [^{3}H]AziP*m* labeling was measured as dpm (disintegrations per minute) per intensity (optical density of the Coomassie-blue stained bands multiplied by the band area in mm^2). Results were analyzed by Mann-Whitney t-test (*, $p<0.05$; mean ± SEM; $n = 4$). (C) Mass spectra of photoaffinity labeled residues V954 (top), and E969 (bottom). (D) Sequence alignment of the S6 helices for mouse TRPA1 (*m*TRPA1), human TRPA1 (*h*TRPA1) and *Drosophila* TRPA1 (*d*TRPA1). Residues photolabeled by AziP*m* in *m*TRPA1, Val954 and Glu969, are indicated in green and with stars.

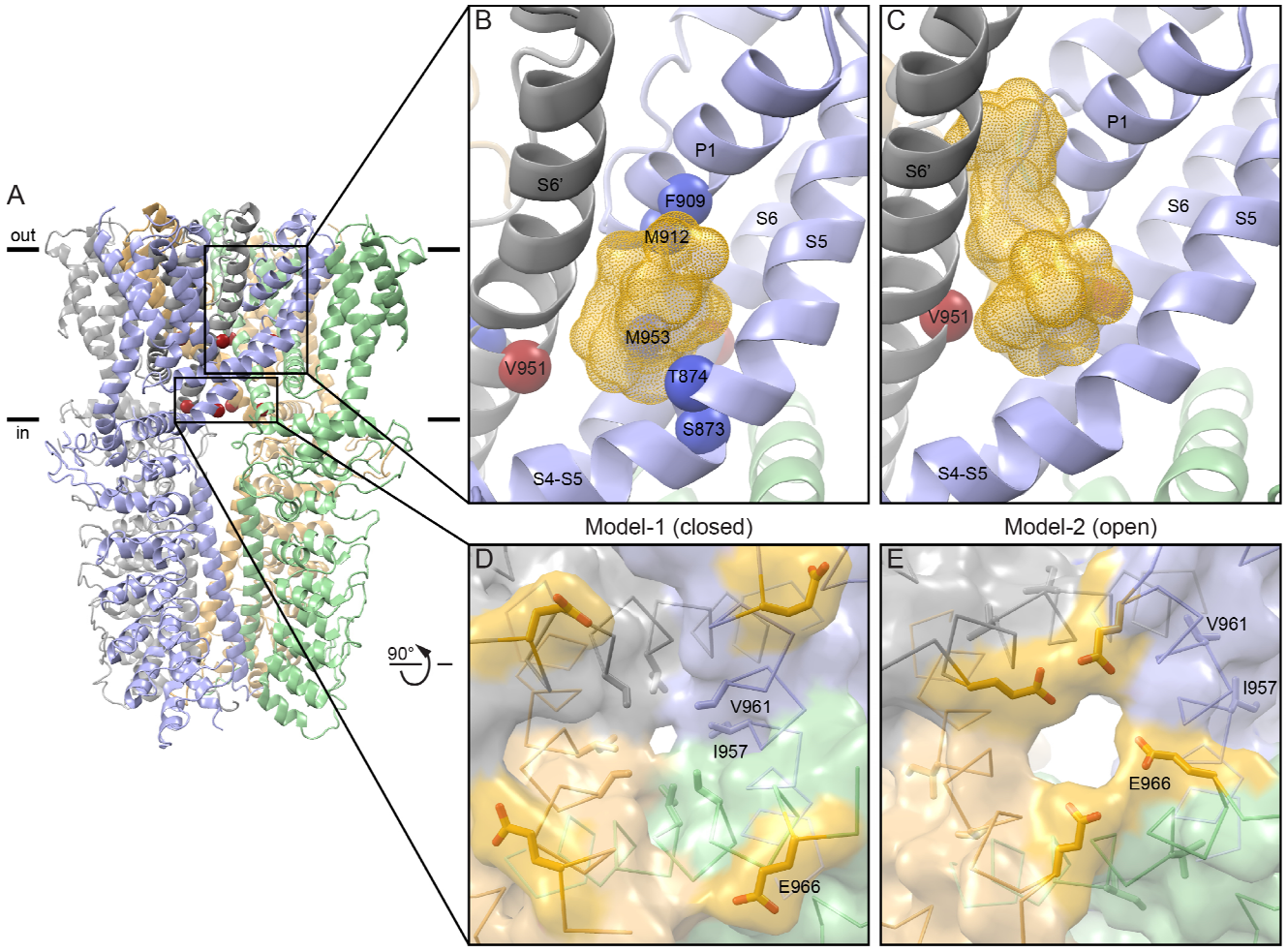

FIGURE 2. Location of photolabeled residues in closed (model-1) and open (model-2) state models of *h*TRPA1. The photolabeled residues V954 and E969 in *m*TRPA1-FLAG align with V951 and E966 in *h*TRPA1 respectively (see Figure 2). (A) Side view of a cartoon representation of the cryo-EM structure of hTRPA1, with the approximate location of the membrane indicated with black bars, each subunit colored a different shade, and the Cα atoms of photolabeled residues shown as red spheres. (B-C) Docking experiments of propofol and AziP*m* in model-1 (B) and model-2 (C). All residues facing cavities were made flexible while backbone structure remained rigid during docking experiments. The yellow dotted Connolly surface representations are of five propofol and five AziP*m* in the highest scored poses predicted by AutoDockVina (26). Red spheres indicate the Cα atoms of V951 (corresponding to V954 photolabeled in *m*TRPA1), and blue spheres the Cα atoms of residues discussed in the main text. (D-E) Cytosolic surface view of the transmembrane domain pore of model-1 (D) and model-2 (E). Lower pore gate residues I957 and V961 are shown as stick representations. E966, corresponding to E969 photolabeled in *m*TRPA1, is shown as yellow stick representation.

SUPPORTING MATERIALS AND METHODS

Sites Contributing to TRPA1 Activation by the Anesthetic Propofol Identified by Photoaffinity Labeling

K. A. Woll,[a] K. A. Skinner,[a] E. Gianti, N. V. Bhanu, B. A. Garcia, V. Carnevale, R. G. Eckenhoff, and R. Gaudet

TABLE OF CONTENTS

Page

SUPPORTING METHODS

Cloning and Expression. Silent mutations a660c and t2163c were introduced into the mouse TRPA1 cDNA (provided by Ardem Patapoutian) to remove two NdeI sites. Full-length TRPA1 was amplified by PCR and ligated between the NdeI and NotI sites of a modified pFastBac1 vector, pFastBac-CFlag, introducing a C-terminal trialanine linker followed by a FLAG-tag (AAADYKDDDDK). Rat TRPV1 baculovirus is previously described [1]. Baculoviruses were generated and used according to standard Bac-to-Bac protocols (Thermo Fischer Scientific, Waltham, MA). Mutants were generated by Quikchange mutagenesis protocol (Stratagene) and all clones were verified by DNA sequencing. Sf21 cells were grown at 27°C in Hink's TNM-FH medium (Mediatech, Manassas, VA) supplemented with 10% fetal bovine serum and 10 μg/mL gentamicin.

Membrane preparation . Sf21 cells (66 mL at 1.25 x 10^6 cells/mL) were infected with mTRPA1-FLAG baculovirus and harvested 48 h post-infection, frozen in liquid nitrogen and stored at -80°C. Membranes were prepared at 4°C. Cells were resuspended and homogenized in 3.5 mL lysis buffer (20 mM HEPES, pH 7.2, 1X Halt Protease Inhibitor Cocktail (Thermo Scientific, Waltham, MA)). Successful lysis was confirmed by visualizing cells under light microscope using Trypan Blue. The homogenate was centrifuged 15 min at 1000 x *g*. The cleared supernatant was centrifuged at 55000 RPM in a Ti90 rotor (Beckman-Coulter, Brea, CA) for 45 min, and the resulting membrane pellets resuspended at 1 mg/mL total protein in lysis buffer and stored in 50 μL aliquots at -80°C.

Calcium-influx assays . Sf21 cells (0.4 x 10^5 cells in 100 μL) were seeded into each well of a 96-well plate, infected with baculovirus and incubated 44-48 h at 27°C. The medium was replaced with 50 μL bath solution (in mM: 150 sodium gluconate, 10 HEPES, 2 $CaCl_2$, 10 NaCl, and 10 D-glucose, 0.02% Pluronic F-127; pH 7.2) containing 5 μM Fura-2-AM. After 45 min, unabsorbed dye was washed away with 180 μL bath solution, replacing with 50 μL of fresh bath solution after 1 h. Experiments were conducted on a Flexstation III (Molecular Devices, Sunnyvale, CA) with excitation at 340/380 nm and emission measured at 510 nm. Test agonists were added at 60 s and 1 mM AITC, 75 nM capsaicin or 1% Triton X-100 was added at 180 s as a positive control for TRPA1, TRPV1 or empty vector, respectively. Compound stocks of tested agonists were made in DMSO and diluted 1:1000 in bath solution immediately before assay measurement. The net change in Fura-2 340/380 fluorescence ratio (ΔRatio) was calculated as the Fura-2 340/380 fluorescence ratio minus the 340/380 ratio of the baseline prior to ligand addition (0-60 s). Data were then averaged after baseline subtraction was performed for each individual trace.

Photoaffinity labeling . Frozen membrane aliquots were thawed on ice before resuspension to 0.5 mg/mL in buffer A (in mM: 50 Tris HCl (pH 7.4), 150 NaCl, 2 CaCl2, 5 KCl, 5 Mg Cl2, 4 EDTA and 250 sucrose) by brief sonication and expulsion through a 27-gauge needle three times. A final concentration of 1 μM [^{3}H]AziP*m* or 1 μM AziP*m* with or without 100 μM propofol was added using methanol or DMSO vehicle (<0.1% v/v%). Membrane suspensions were gently mixed and equilibrated on ice in the dark for 5 min. Samples were irradiated for 25 min at 350 nm 3 cm from light source in a 1-mm pathlength quartz cuvette through a 295 nm low pass filter.

Immunopurification of TRPA1-FLAG channels . Irradiated membrane preparations were diluted to 0.25 mg/mL with a final concentration of 6.25 mM n-dodecyl-β-D-maltoside (DDM) in buffer A containing protease and phosphatase inhibitors. Membranes were solubilized by gentle rocking for 4 hr, in the dark, at 4 °C. These samples were diluted to 0.1 mg/mL and a final DDM concentration of 2.5 mM with buffer A containing protease and phosphatase inhibitors equilibrated for 2 hrs, in the dark, at 4°C before centrifugation at 16,000 x g for 20 min at 4°C to remove insoluble debris. ANTI-FLAG M2 Affinity Gel (Sigma) was equilibrated with one wash of buffer A without sucrose, then two washes of buffer A, and finally two washes of buffer A containing 2.5 mM DDM, 20 resin volumes each. Equilibrated 20 μL ANTI-FLAG® M2 Affinity Gel was added to each solubilized membrane preparation. Samples were incubated in the dark overnight with gentle over-end mixing at 4°C. The resin was washed three times with 20 volumes of buffer A containing 75 μM DDM. TRPA1-FLAG was eluted from resin by the addition of 2X SDS buffer before separation by SDS-PAGE. Gels were stained with Coomassie blue G-250, destained, and thoroughly washed with ddH_2O.

Scintillation counting- Gels were scanned on a Bio-Rad GS-800 calibrated densitometer with quantitation performed using the accompanying Quantity One software. Background was subtracted with a box drawn between the 100- and 150-kDa molecular mass markers, and mean optical density multiplied by band area was recorded from excised band regions. Excised bands were placed into scintillation vials containing 1 mL of 30% hydrogen peroxide and incubated overnight at 65°C to dissolve the polyacrylamide. Samples were cooled to room temperature before adding 10 mL EcoLite(+) liquid

scintillation mixture (MP Biomedicals). Samples were analyzed using PerkinElmer Life Sciences Tri-Carb 2800TR instrument.

In-gel protease digestion. Identified protein bands at ~110-140kDa, corresponding to TRPA1-FLAG, were excised, destained, dehydrated and dried by SpeedVac before proteins were reduced by incubation at 56°C for 20 min in 25 mM dithiothreitol (DTT) and 50 mM NH_4HCO_3. The DTT solution was removed and proteins were then alkylated by the addition of 55 mM iodoacetamide in 50 mM NH_4HCO_3 and incubation at room temperature in the dark. Bands were dehydrated and dried by SpeedVac before resuspension in 100 µL 0.2 % ProteaseMAX™ Durfactant (Promega), 1 mM $CaCl_2$ and 50 mM NH_4HCO_3 solution containing sequencing grade trypsin (Promega) at a 1:20 protease:protein ratio (w/w). Proteins were digested overnight at 37°C. After, samples were diluted to 200 µL with final concentration of 100 mM NH_4HCO_3 and 0.2% ProteaseMAX™ Surfactant prior to the addition of sequencing grade chymotrypsin (Promega) to a final 1:20 protease:protein ratio (w/w). Proteins were digested overnight at 37°C. To increase hydrophobic peptide retrieval from the gel, multiple peptide extractions were performed. First the initial peptide digest solution was removed and 100 µL 30% acetylnitrile (ACN) and 5% acetic acid in ddH_2O (v/v%) was added. Samples were sonicated for 20 min. The second peptide extraction was removed before 100 µL 70% ACN and 5% acetic acid in ddH_2O (v/v%) was added. Samples were sonicated for 20 min. All peptide digests were pooled and dried by SpeedVac before resuspension in 0.5% acetic acid and desalting using C18 stage tips prepared in house. Samples were dried by SpeedVac and resuspended in 0.1% formic acid immediately prior to mass spectrometry analysis.

Mass spectrometry. Desalted peptides were analyzed on an Orbitrap Elite™ Hybrid Ion Trap-Orbitrap Mass Spectrometer (MS) coupled to an Easy-nanoLC 1000 system with a flow rate of 300 nL/min. Peptides were eluted with 100 min with linear gradients of ACN in 0.1% formic acid in water (v/v) starting from 2% to 40% (85 min), then 40% to 85% (5 min) and finally 85% (10 min). Data dependent acquisition mode was applied with a dynamic exclusion of 45 s. In every 3 s cycle, one full MS scan was collected with a scan range of 350 to 1500 m/z, a resolution of 60K and a maximum injection time was 50 ms and automatic gain (AG) control of 500000. The MS2 scans were followed from the most intense parent ions. Ions were filtered with charge 2-5 with an isolation window of 1.5 m/z in quadruple isolation mode. Ions were fragmented using collision induced dissociation (CID) with collision energy of 35%. Iontrap detection was used with normal scan range mode and rapid iontrap scan rate. AG was set to be 10000 with a maximal injection time of 100 ms.

Mass spectrometry analysis. Spectral analysis was conducted using Thermo Proteome Discoverer 2.0 (Thermo Scientific) and the Mascot Daemon search engine using a customized database containing *m*TRPA1-AAA-FLAG sequences supplied for heterologous expression. All analyses included dynamic oxidation of methionine (+15.9949 *m/z*) and static alkylation of cysteine (+57.0215 *m/z*; iodoacetamide alkylation). Photolabeled samples were run with the additional dynamic AziP*m* (+216.1996 *m/z*) modification. A mass variation tolerance of 10 ppm for MS and 0.8 Da for MS/MS were used. The in-gel sequential trypsin/chymotrypsin digests were searched without enzyme specification with a false discovery rate of 0.01%. Samples were conducted in triplicate and samples containing no photoaffinity ligand were treated similarly to control for false positive detection of photoaffinity ligand modifications.

Molecular modeling. The electron density (4.24 Å resolution) obtained via single particle cryo-electron imaging of human TRPA1 (PDB ID: 3J9P) [2] did not provide enough structural information to confidently model the full-length protein. Therefore, prior to any docking simulations, we generated two structures with all missing linkers reconstructed of human TRPA1 as models of the intermediate-closed (model-1) and open (model-2) states of the channel. The multistep procedure consisted of: (i) generation of initial structural models by comparative homology modeling using Modeller (v. 9.16) [3]; (ii) model selection using clustering [4]; (iii) optimization of side chains rotamers using SCWRL4 [5]. For model-1, the templates were taken from the cryo-electron microscopy structures for human TRPA1 (PDB ID: 3J9P)[2] and TRPV1 (PDB ID: 5IRX) [6]. A multiple sequence alignment containing the templates and the full-length sequence of human TRPA1 (UniProt code: O75762) was generated using PROMALS3D [7] and EMBOSS [8]. We then generated a pool of 6032 models and selected the most representative one by combining multiple criteria: clustering (choosing the central structure of the most populated clusters), DOPE score (lowest values) and visual inspection. We then optimized the rotameric state of all the side chains using SCWRL4 [5]. For model-2, we adopted an analogous protocol, except for the templates: in this case we used the structure of the open state of TRPV1 (PDB ID: 5IRX) and limited the model to the transmembrane region. We generated an initial pool of 500 models and the top structure was selected and optimized as described above.

Docking. Generated model-1 and model-2 for TRPA1 were used for docking experiments. Ions and crystallographic ligands were removed by PyMOL [9]. AutodockTools4 [10] was used to add hydrogens and Kollman charges, merge nonpolar hydrogen, and define flexible residues. Molecular coordinates for propofol were downloaded from the ZINC small molecule library [11] using provided physical representations. The molecular coordinates for AziP*m* were generated using MarvinSketch version 16.3.28.0 and AutodockTools4 to generate geisteiger charges and to merge nonpolar hydrogens. The maximum torsions were allowed for propofol and AziP*m* respectively (i.e., ligands were fully flexible). Separate docking simulations using AutoDock Vina [12] were performed similar to as previously reported [13,14] of the entire accessible TMD interface cavities formed by three TRPA1 monomers. The grid box dimensions were 32x28x32 for model-1 and 32x26x32 model-2 at 1Å resolution and contained both S4-S5 [15] and S5-S6 pockets (A-967079 binding site) [2] as well as the width of the TMD region. All cavity facing residue side-chains were made flexible. Images and distance measurements were prepared using PyMOL.

Statistics. GraphPad Prism 7 or Microsoft Excel was used for preparation of graphs and statistical analysis. All p-values are reported in the figures and figure legends, as appropriate.

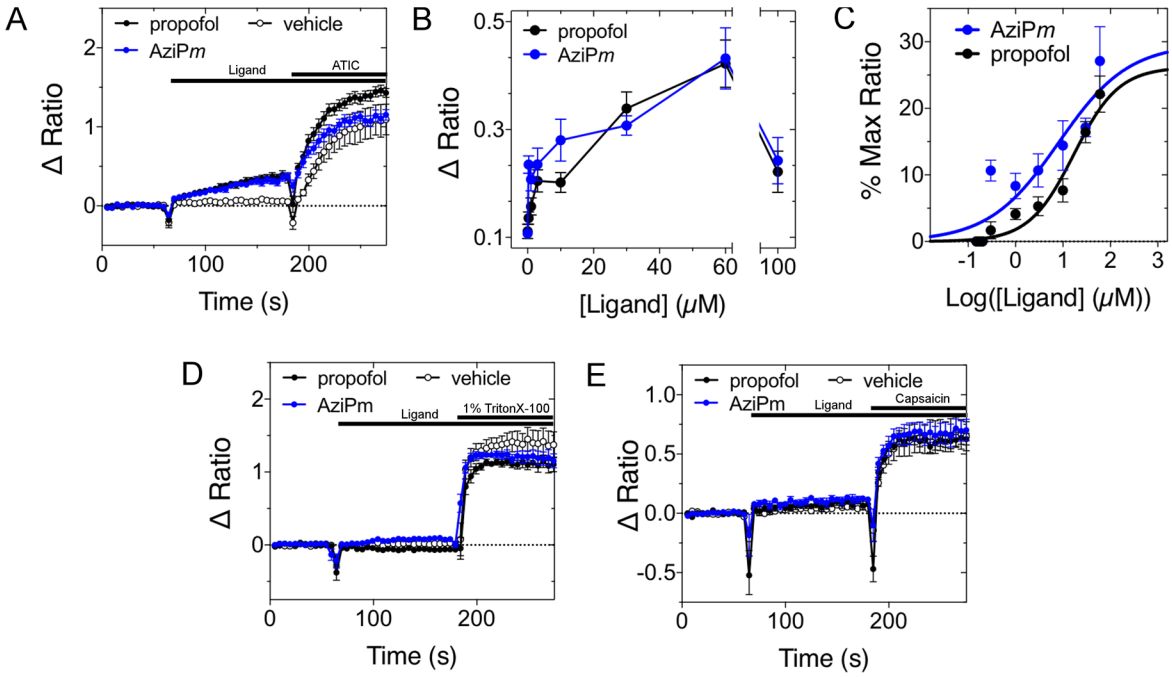

Fig. S1. AziP*m* and propofol cause calcium influx TRPA1 and not in control or TRPV1 heterologously expressed in Sf21 cells. (A) Net change in Fura-2 340/380 fluorescence ratio (ΔRatio) with 60 μM propofol or AziP*m* or vehicle control added at 60 s. Addition of 1 mM allyl isothiocyanate (AITC) at 180 s provided a positive control for TRPA1 expression. Data represent mean ± SEM (n = 9). (B) Dose-dependent net change in Fura-2 340/380 fluorescence ratio (ΔRatio) with varying concentrations of propofol and AziP*m* (n= 9-12). (C) Concentration-response curves of $[Ca^{2+}]_i$ responses to propofol or AziP*m*, plotting the percent net change in Fura-2 340/380 fluorescence ratio of a mean maximum allyl isothiocyanate response. Lines represent the best-fit sigmoidal dose-response curves with variable slope with the minimum and maximum values constrained to 0 and <40% respectively. Points represent mean ± SEM (*n*= 9-12). (D) AziP*m* and propofol do not cause non-specific calcium fluxes. AziP*m* or propofol (100 μM) at 60 s did not elicit a rise in $[Ca^{2+}]_i$ in empty vector-infected insect cells. Addition of 1% Triton X-100 detergent at 180 s did cause large increases in the 340/380 ratio, confirming that the cells were effectively loaded with Fura-2. Data represent mean ± SEM for n=6. (E) AziP*m* and propofol did not activate rat TRPV1. Addition of 100 μM AziP*m* or propofol at 60s did not elicit a rise in $[Ca^{2+}]_i$ in rat TRPV1-expressing insect cells. Capsaicin, a TRPV1-specific agonist added at 180 s, did elicit a rise in $[Ca^{2+}]_i$ thus confirming TRPV1 expression in all samples. Data represent mean ± SEM for n=6.

MKRGLR**RILL PEERKEVQGV VYRGVGEDMD CSKESFKVDI EGDMCRLEDF IKNRRKLSKY**
EDENLCPLHH AAAEGQVELM ELIINGSSCE VLNIMDGYGN TPLHCAAEKN QVESVKFLLS
QGANPNLRNR NMMSPLHIAV HGMYNEVIKV LTEHKATNIN LEGENGNTAL MSTCAK**DNSE**
ALQILLEKGA KLCKSNKWGD YPVHQAAFSG AKKCMELILA YGEKNGYSRE THINFVNHKK
ASPLHLAVQS GDLDMIKMCL DNGAHIDMME NAKCMALHFA ATQGATDIVK LMISSYTGSS
DIVNAVDGNQ ETLLHRASLF DHHDLAEYLI SVGADINSTD SEGRSPLILA TASASWNIVN
LLLCKGAKVD IKDHLGRNFL HLTVQQPYGL RNLRPEFMQM QHIKELVMDE DNDGCTPLHY
ACRQGVPVSV NNLLGFNVSI HSKSKDKKSP LHFAASYGRI NTCQRLLQDI SDTRLLNEGD
LHGMTPLHLA AKNGHDKVVQ LLLKKGALF**L SDHNGWTALH HASMGGYTQT MKVILDTNLK**
CTDRLDEEGN TALHFAAREG HAK**AVAMLLS YNADILLNKK QASFLHIALH NKRKEVVLTT**
IRNKRWDECL QVFTHNSPSN RCPIMEMVEY LPECMKVLLD FCMIPSTEDK SCQDYHIEYN
FKYLQCPLSM TKKVAPTQDV VYEPLTILNV MVQHNRIELL NHPVCREYLL MKWCAYGFRA
HMMNLGSYCL GLIPMTLLVV KIQPGMAFNS TGIINGTSST HEERIDTLNS FPIKICMILV
FLSSIFGYCK EVIQIFQQKR NYFLDYNNAL EWVIYTTSII FVLPL**FLNIP AYMQWQCGAI**
AIFFYWMNFL LYLQRFENCG IFIVMLEVIF KTLLRSTGVF IFLLLAFGLS FYVLLNFQDA
FSTPLLSLIQ TFSMMLGDIN YRDAFLEPLF RNELAYPVLT FGQLIAFTMF VPIVLMNLLI
GLAVGDIAEV QKHASLKRIA MQVELHTNLE KKLPLWYLRK VDQRSTIVYP NRPRHGRMLR
FFHYFLNMQE TRQEVPNIDT CLEMEILKQK YRLKDLTSLL EKQHELIKLI IQKMEIISET
EDEDNHCSFQ DRFKKERLEQ MHSKWNFVLN AVKTKTHCSI SHPDFAAADY KDDDDK

Fig. S2. Coverage map for TRPA1 mass spectrometry analysis. Sequence of the purified *m*TRPA1-AAA-FLAG with high confidence coverage in the mass spectrometry analysis denoted as black residue codes (representing 92.96% coverage).

A

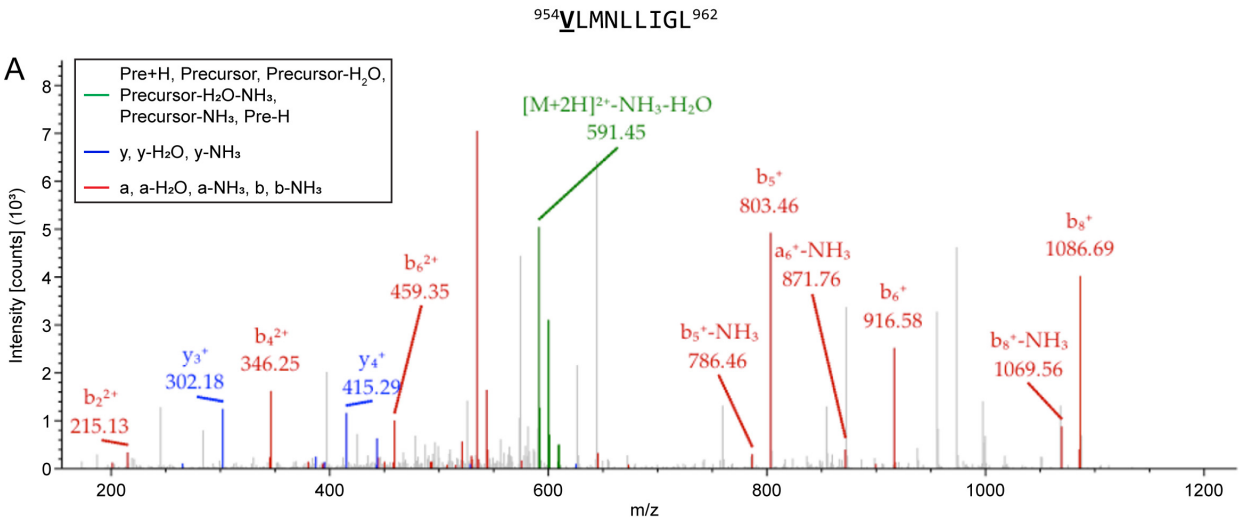

B

#1	a⁺	a²⁺	b⁺	b²⁺	Seq.	y⁺	y²⁺	#2
1	288.15698	144.58213	316.15190	158.57959	**V-AziPm**			9
2	401.24105	201.12416	429.23597	215.12162	L	902.53801	451.77264	8
3	548.27647	274.64187	576.27138	288.63933	M-Oxidation	789.45394	395.23061	7
4	662.31940	331.66334	690.31431	345.66079	N	642.41852	321.71290	6
5	775.40347	388.20537	803.39838	402.20283	L	528.37559	264.69143	5
6	888.48754	444.74741	916.48245	458.74486	L	415.29152	208.14940	4
7	1001.57161	501.28944	1029.56652	515.28690	I	302.20745	151.60736	3
8	1058.59308	529.80018	1086.58799	543.79763	G	189.12338	95.06533	2
9					L	132.10191	66.55459	1

Fig. S3. Identification of AziPm adduct at V954 within the ^{954}**V**LMNLLIGL^{962} peptide fragment. (A) Mass spectrum of the ^{954}**V**LMNLLIGL^{962} peptide, which contains an AziP*m* adduct at V954. (B) Fragment table showing the fragmentation of the ^{954}**V**LMNLLIGL^{962} photolabeled peptide. Detected identified a, b (red) and y (blue) ions are colored red and blue, respectively. Residues detected with a modification are noted, and the one modified by AziPm additionally noted in bold and underlined.

A

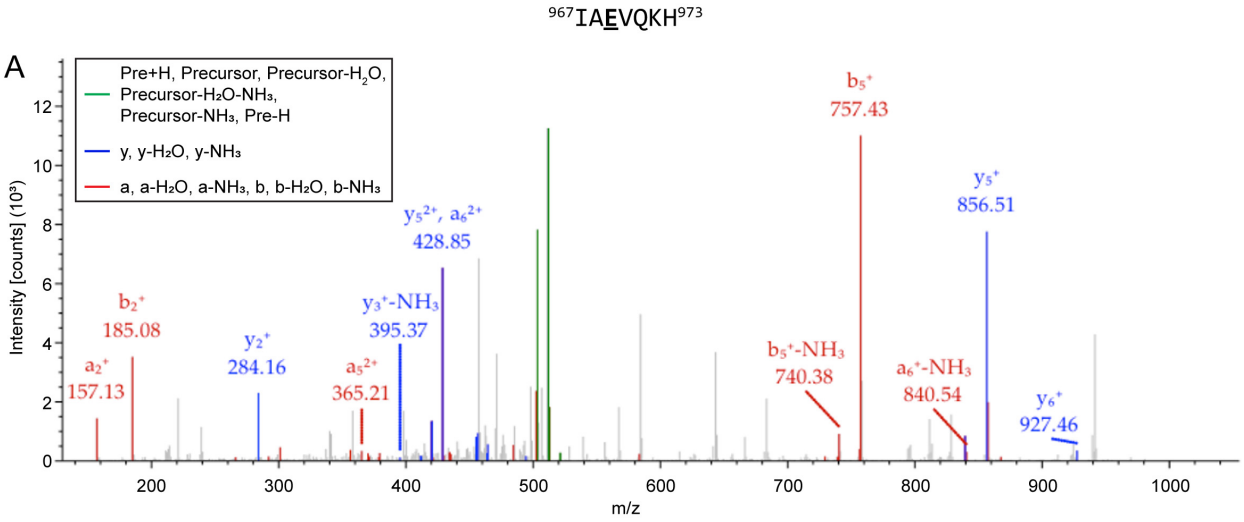

B

#1	a⁺	a²⁺	b⁺	b²⁺	Seq.	y⁺	y²⁺	#2
1	86.09643	43.55185	114.09135	57.54931	I			7
2	157.13355	79.07041	185.12847	93.06787	A	927.45464	464.23096	6
3	502.25235	251.62981	530.24727	265.62727	**E-AziPm**	856.41752	428.71240	5
4	601.32077	301.16402	629.31569	315.16148	V	511.29872	256.15300	4
5	729.37935	365.19331	757.37427	379.19077	Q	412.23030	206.61879	3
6	857.47432	429.24080	885.46924	443.23826	K	284.17172	142.58950	2
7					H	156.07675	78.54201	1

Fig. S4. Identification of AziPm adduct at E969 within the ^{967}IA**E**VQKH^{973} peptide fragment. (A) Mass spectrum of the ^{967}IA**E**VQKH^{973} peptide, which contains an AziP*m* adduct at E969. (B) Fragment table showing the fragmentation of the ^{967}IA**E**VQKH^{973} photolabeled peptide. Detected identified a, b (red) and y (blue) ions are colored red and blue, respectively. Residues detected with a modification by AziPm is noted in bold and underlined.

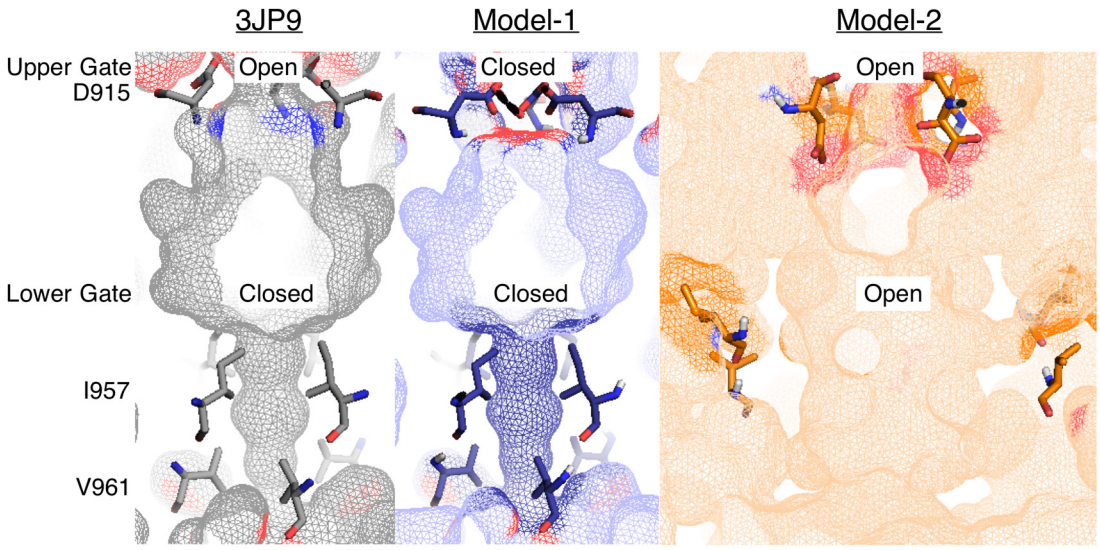

Fig. S5. Gate and pore conformations for the TRPA1 cryo-EM structure, model-1 and model-2. Illustrations of the TRPA1 pore and upper and lower gates of human TRPA1 cryo-EM structure (PDB: 3PJ9) (gray), model-1(blue) and model-2 (orange). Upper gate residue D915 and lower pore gate residues I957 and V961 are shown as stick representations. The mesh surface representation shows the pore diameter in each model.

SUPPORTING REFERENCES

1. Lishko, P. V, Procko, E., Jin, X., Phelps, C. B. & Gaudet, R. The ankyrin repeats of TRPV1 bind multiple ligands and modulate channel sensitivity. *Neuron* **54,** 905–918 (2007).
2. Paulsen, C. E., Armache, J.-P., Gao, Y., Cheng, Y. & Julius, D. Structure of the TRPA1 ion channel suggests regulatory mechanisms. *Nature* **520,** 511–517 (2015).
3. Eswar, N. *et al.* in *Current Protocols in Bioinformatics* (eds. Bateman, A., Pearson, W. R., Stein, L. D., Stormo, G. D. & Yates, J. R.) 5.6.1-5.6.30 (John Wiley & Sons, Inc., 2006).
4. Pronk, S. *et al.* GROMACS 4.5: a high-throughput and highly parallel open source molecular simulation toolkit. *Bioinformatics* **29,** 845–854 (2013).
5. Krivov, G. G., Shapovalov, M. V. & Dunbrack, R. L. Improved prediction of protein side-chain conformations with SCWRL4. *Proteins* **77,** 778–795 (2009).
6. Gao, Y., Cao, E., Julius, D. & Cheng, Y. TRPV1 structures in nanodiscs reveal mechanisms of ligand and lipid action. *Nature* **534,** 347–351 (2016).
7. Pei, J., Kim, B.-H. & Grishin, N. V. PROMALS3D: a tool for multiple protein sequence and structure alignments. *Nucleic Acids Res.* **36,** 2295–2300 (2008).
8. Rice, P., Longden, I. & Bleasby, A. EMBOSS: the European Molecular Biology Open Software Suite. *Trends Genet. TIG* **16,** 276–277 (2000).
9. Schrödinger, LLC. *The {PyMOL} Molecular Graphics System, Version~1.8*. (2015).
10. Morris, G. M. *et al.* AutoDock4 and AutoDockTools4: Automated Docking with Selective Receptor Flexibility. *J. Comput. Chem.* **30,** 2785–2791 (2009).
11. Irwin, J. J., Sterling, T., Mysinger, M. M., Bolstad, E. S. & Coleman, R. G. ZINC: A Free Tool to Discover Chemistry for Biology. *J. Chem. Inf. Model.* **52,** 1757–1768 (2012).
12. Trott, O. & Olson, A. J. AutoDock Vina: improving the speed and accuracy of docking with a new scoring function, efficient optimization, and multithreading. *J. Comput. Chem.* **31,** 455–61 (2010).
13. Jayakar, S. S. *et al.* Multiple Propofol Binding Sites in a gamma-Aminobutyric Acid Type A Receptor (GABAAR) Identified Using a Photoreactive Propofol Analog. *J Biol Chem* **1,** 581728 (2014).
14. Woll, K. A. *et al.* Photoaffinity ligand for the inhalational anesthetic sevoflurane allows mechanistic insight into potassium channel modulation. *ACS Chem. Biol.* (2017). doi:10.1021/acschembio.7b00222
15. Brewster, M. S. J. & Gaudet, R. How the TRPA1 receptor transmits painful stimuli: Inner workings revealed by electron cryomicroscopy. *Bioessays* **37,** 1184–1192 (2015).